Band structure and absorption properties of $GaAs_{1-x}N_x/InAs_{1-y}N_y$ short period superlattices strained to InP (001)

L. Bhusal and A. Freundlich*

Photovoltaics and Nanostructures Laboratories, Center for Advanced Materials and Physics Department, University of Houston, Houston, Texas 77204-5004, USA

(Received 8 December 2005; revised manuscript received 5 October 2006; published 13 February 2007)

The $\boldsymbol{k}\cdot\boldsymbol{p}$ approximation and the band anticrossing model modified for the strain are used to describe the electronic states of the strained bulk $GaAs_{1-x}N_x$ and $InAs_{1-y}N_y$ ternaries in the vicinity of the center of the Brillouin zone (Γ point) and their respective band offsets have been evaluated, before implementing them into the superlattice structure. By minimizing the total mechanical energy of the stack of the alternating layers of $GaAs_{1-x}N_x$ and $InAs_{1-y}N_y$ in the superlattice, the ratio of the thicknesses of the epilayers is determined to make the structure lattice matching on InP(001). Energy miniband structure of the superlattice is then investigated using the transfer-matrix formalism, predicting the evolution of the band-edge transition energies for different nitrogen concentrations and thickness combinations. The results show the potential to significantly reduce the band gap compared to quaternary alloys of similar average concentration and to obtain photon absorption and emission energies in the range of 0.65–0.35 eV at 300 K for a typical nitrogen concentration of $\leq 5\%$. Finally, the optical-absorption coefficient of such a superlattice, as a function of the nitrogen concentration, the change in electron effective masses, and the temperature are estimated under the anisotropic medium approximation.

DOI: 10.1103/PhysRevB.75.075321 PACS number(s): 73.40.Kp, 73.21.Cd, 73.61.Ey, 78.67.Pt

I. INTRODUCTION

It has been long known that a small quantity of nitrogen in GaAs and GaP forms a deep level impurity.[1] However, the unusual large band-gap lowering observed in (In)$GaAs_{1-x}N_x$ with low nitrogen fraction[2,3] has sparked a new interest in the development of dilute nitrogen containing III-V semiconductors for long-wavelength optoelectronic devices (e.g., IR lasers, detectors, solar cells).[3–7] Thus far most of the work had been concentrated on the development of (In)GaAsN alloys lattice-matched to the GaAs substrate.[1–6] Theoretically, the band gap of $GaAs_{1-x}N_x$ can be further reduced by subjecting it to a biaxial tensile strain, e.g., by fabricating pseudomorphically strained layers on commonly available InP substrates. While such an approach, in principle, could allow access to smaller band gap (longer wavelength), only a few atomic monolayers of the material can be grown due to the large lattice mismatch between $GaAs_{1-x}N_x$ and InP ($\sim$3.8–4.8 % for $x<0.05$, 300 K). This limitation can be circumvented using the principle of strain balancing,[8–11] by introducing alternating layers of $InAs_{1-y}N_y$ with opposite strain ($\sim$2.4–3.1 % for $x<0.05$, 300 K) in combination with $GaAs_{1-x}N_x$. Therefore a pseudomorphically strained superlattice (Fig. 1) can be realized from a sequence of $GaAs_{1-x}N_x$ and $InAs_{1-y}N_y$ layers if the thickness of each layer is kept below the threshold for its lattice relaxation. In such a short-period superlattice, carrier wave function in the given well layer penetrates deep into the other neighboring well layers in the growth direction, if the barrier material is thin. The effect of this encroachment of the wave function can be treated assuming the anisotropy is introduced by the layers along the growth direction. In other words, a short-period superlattice can be assumed as being made up of a material that has different properties along the growth direction and the direction perpendicular to the growth. The amount of anisotropy would depend on the amount of wave-function encroachment in the neighboring layers. The thicker the barrier layer, the smaller the penetration and the higher the anisotropy would be. On the other hand if the barrier layer is very thin, the wave function will be smooth across the structure, which is equivalent to the bulk, and hence the structure will be isotropic along the growth direction and the direction perpendicular to the growth. This anisotropy will change the effective mass of the carriers in two perpendicular directions and the anisotropy factor, defined as the ratio of the reduced effective masses along the plane and perpendicular to the superlattice layers, can be used to find the variation in the

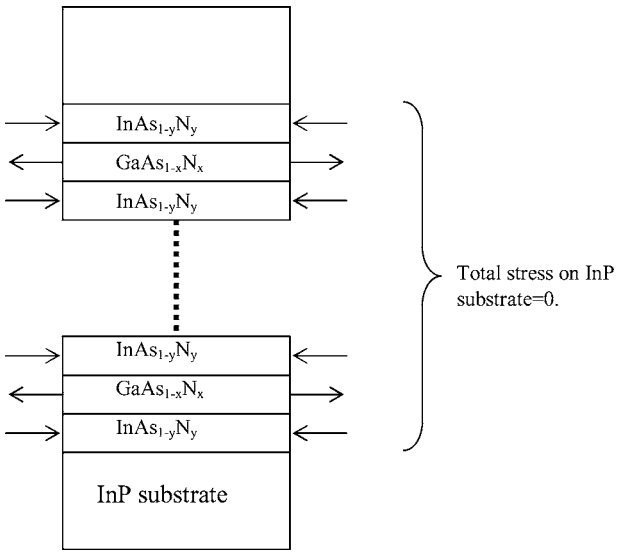

FIG. 1. Schematic of the strain-balanced superlattice on InP substrate. Converging and diverging arrows show the compressive and tensile stresses on the layers, respectively. Stresses on each layer, being opposite in nature, cancel each other, producing a total of zero stress on the substrate.

absorption coefficients of the superlattice in comparison to the bulk.

In this work, along with the calculations of the electronic band structure of the individual strained $InAs_{1-y}N_y$ and $GaAs_{1-x}N_x$ layers and the conditions for the strain balancing to create a $GaAs_{1-x}N_x/InAs_{1-y}N_y$ short-period superlattice lattice matched on InP(001), the electronic band structure of such a superlattice for different combinations of nitrogen concentrations x and y is investigated. The evolution of the optical-absorption coefficient of the superlattice as a function of the temperature, effective masses, and the nitrogen concentration is also analyzed.

The paper is organized as follows: in Sec. II we will discuss the strain-balancing concept and conditions for a $GaAs_{1-x}N_x/InAs_{1-y}N_y$ superlattice structure with an estimate of monolayer ratio to create a strain balancing. In Sec. III we will discuss the band-structure calculation formalism for conduction and valence bands for III-V-N near the Γ point, with calculation results for $GaAs_{1-x}N_x$ and $InAs_{1-y}N_y$. In Sec. IV, the transfer-matrix technique is used to calculate the effective band gap of the $GaAs_{1-x}N_x/InAs_{1-y}N_y$ for different combinations of x and y. Finally, before the conclusions we will present an optical-absorption coefficient formalism and results for the superlattice using the anisotropy in the structure in Sec. V.

II. STRAIN BALANCING

If the misfit between a bulk substrate and a grown epilayer is sufficiently small, first atomic layers that are deposited will be strained to match the substrate, and a coherent (or pseudomorphic) interface will be formed. However, as the epilayer thickness increases, the homogenous strain energy becomes so large that a critical thickness is reached where it becomes favorable for misfit dislocations to be introduced.[12,13] By balancing the stresses in one compressively strained layer by another tensilely strained layer, the stack of layers can be engineered to have nearly zero total stress on the substrate. In principle, to get a strain-balanced structure, the tensile and compressive layers should be pseudomorphically strained to the substrate of crystalline nature. One way to achieve the relation for thickness of the two adjacent layers strain balancing each other is by minimizing the energy density with respect to the strain in one layer. The elastic strain energy of the layer can be written in terms of the stress and strain tensors σ_{ij} and ε_{ij}, respectively, as[14]

$$E = \frac{1}{2}\int_V \sum_{i,j} \sigma_{ij}\varepsilon_{ij} dV, \tag{1}$$

where $i,j=x,y,z$ are the three Cartesian directions. For a cubic symmetry in (001) orientation, Hook's law provides the following three equations:[14]

$$\sigma_{xx} = C_{11}\varepsilon_{xx} + C_{12}\varepsilon_{yy} + C_{12}\varepsilon_{zz},$$

$$\sigma_{yy} = C_{12}\varepsilon_{xx} + C_{11}\varepsilon_{yy} + C_{12}\varepsilon_{zz},$$

$$0 = C_{12}\varepsilon_{xx} + C_{12}\varepsilon_{yy} + C_{11}\varepsilon_{zz}, \tag{2}$$

where C_{11} and C_{12} are the elastic stiffness constants. For the biaxial stress in the plane of an epilayer, the strain components in the epilayer are given as

$$\varepsilon_{xx} = \varepsilon_{yy} = \frac{a_0 - a_a}{a_a} = \varepsilon_{\parallel}, \tag{3}$$

where a_a and a_0 are the in-plane lattice constants of the epilayer and the substrate, respectively. Using the third equation of the equation set (2), we have

$$\varepsilon_{zz} = \varepsilon_{\perp} = -\frac{2C_{12}}{C_{11}}\varepsilon_{\parallel}. \tag{4}$$

Using Eqs. (1)–(4), the energy density (energy per unit volume) of the strained epilayer is

$$U = \frac{1}{2}C_{11}(\varepsilon_{xx}^2 + \varepsilon_{yy}^2 + \varepsilon_{zz}^2) + C_{12}(\varepsilon_{xx}\varepsilon_{zz} + \varepsilon_{zz}\varepsilon_{xx} + \varepsilon_{xx}\varepsilon_{yy})$$

$$= \left(C_{11} + C_{12} - \frac{2C_{12}^2}{C_{11}}\right)\varepsilon_{\parallel}^2 = G\varepsilon_{\parallel}^2, \tag{5}$$

where the constant G, in the chosen [001] direction, is given as $(C_{11}+C_{12}-2C_{12}^2/C_{11})$ and would be different in other directions. For a strained layer superlattice made up of two zinc-blende structure materials, the strain energy density is given as

$$U_{AB} = \frac{U_A t_B + U_B t_A}{t_A + t_B}, \tag{6}$$

where t_A and t_B are the thicknesses of the two respective layers. Minimizing the total energy with respect to the strain in a given layer, for a superlattice fabricated from alternating layers of materials A and B, the condition for zero in-plane stress or the condition for strain balancing requires[15,16]

$$\frac{t_A}{t_B} = -\frac{\varepsilon_B G_B a_A}{\varepsilon_A G_A a_B}, \tag{7}$$

where a_A and a_B are the lattice constants of material layers A and B, respectively, G is a constant defined in Eq. (5), and the strain component ε is defined in Eq. (3).

For semiconductors alloys of interest and for relatively small nitrogen concentrations $(x,y<0.05)$ the average strain in individual layers when strained to InP ranges from 3 to 5 %, and in order to prevent lattice strain relaxation, by analogy to experimental data for materials systems with similar lattice mismatches and elastic constants like GaP or InP on GaAs (Ref. 8) and InAs on InP, the thickness of individual layers has to be maintained below 4 and 7 monolayers for GaAsN and InAsN, respectively. The evaluation of the critical thickness introduced by Van der Merwe,[17] Matthews and Blakeslee,[18] and Bean and People[13] provide critical thickness that often differs by order of magnitude and most often are applicable for only a finite range of strain. In addition, it has been shown that for the epitaxial synthesis of thin films the growth kinetics (temperature, deposition rates) play an important role in determining the critical thicknesses for given epistructures, an example of such dependence is provided by

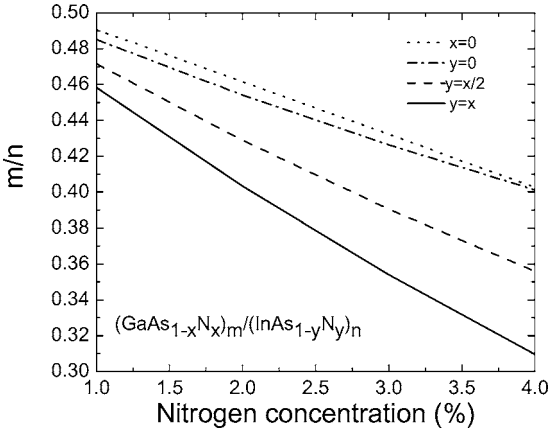

FIG. 2. Ratio of the numbers of monolayers (MLs) (m/n) of $GaAs_{1-x}N_x$ and $InAs_{1-y}N_y$ required to strain-balance the $(GaAs_{1-x}N_x)_m/(InAs_{1-y}N_y)_n$ superlattice on InP for different nitrogen concentrations and different combinations of x and y.

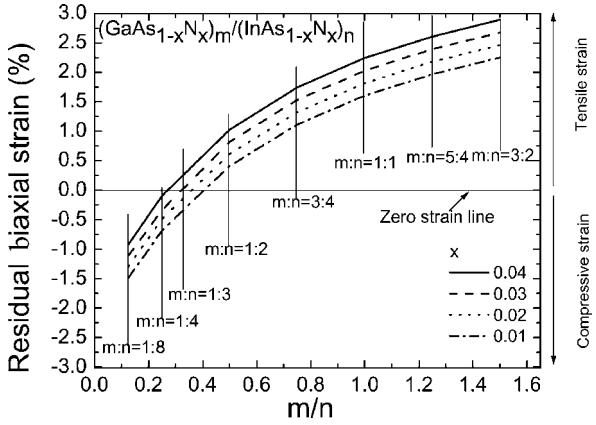

FIG. 3. Residual in-plane biaxial strain on InP for different $GaAs_{1-x}N_x$ and $InAs_{1-x}N_x$ monolayers thickness ratios in $(GaAs_{1-x}N_x)_m/(InAs_{1-x}N_x)_n$ superlattice and different nitrogen concentrations. Vertical lines show different combinations of ratio m/n.

Price.[19] Thus from a practical standpoint the critical thickness is generally extracted empirically. It is worth noting that, for materials considered here, the analogy to experimental data for materials systems with merely similar lattice mismatches and elastic constants provides a relatively good estimate of the lower limit of the critical thicknesses at play, since an enhancement of the biaxial modulus and of the energy of the formation of dislocations are expected through nitrogen alloying (e.g., see Refs.13 and 17). We have thus limited the boundary of our study to the range of thicknesses where in principle two-dimensional defect-free structures are likely to be realized.

When the above-mentioned condition is respected, one using the condition described in Eq. (7) can evaluate the necessary average thickness-ratio condition for strain balancing. Figure 2 shows the variation of the ratio of the numbers of monolayers of $(GaAs_{1-x}N_x)_m$ and $(InAs_{1-y}N_y)_n$ required to obtain exact strain balancing to InP(001) for different nitrogen concentrations. When strained to InP, increasing nitrogen concentration increases the tensile strain of the $GaAs_{1-x}N_x$ layer, while the compressive strain on the $InAs_{1-y}N_y$ layer decreases. Thus a thicker $InAs_{1-y}N_y$ layer is needed to produce strain balancing, hence the ratio $m:n$ to produce exact strain balancing decreases with increasing nitrogen concentration. The magnitude of the ratio $m:n$, of course, is a function of individual nitrogen concentrations x and y in $GaAs_{1-x}N_x$ and $InAs_{1-y}N_y$ sublayers. For illustrative purposes in Fig. 2, several arbitrary nitrogen concentrations are represented. For practical applications, fabrication (growth) of partial monolayers to produce exact strain balancing may not be easy to control or desirable (due to the interface roughness and scattering). Residual biaxial strain is developed on the substrate if the in-plane lattice constant of the superlattice, resulting from the energy minimization, is not the same as that of the substrate [residual strain $=(a_{substrate}-a_{superlattice})/a_{substrate}$]. Figure 3 shows the variation of residual biaxial strain on the InP substrate due to the nonstrain balanced $GaAs_{1-x}N_x/InAs_{1-y}N_y$ superlattice for different nitrogen concentrations. The intersection of the vertical lines with the curves of different nitrogen concentrations gives the amount of the residual strain for the exact fractional ratio of the monolayers (viz., $m:n=1:8$, 1:4, 1:3, 1:2, 3:4, 1:1, 5:4, 3:2). On the other hand, the intersection of the horizontal zero-strain line with the curves of different nitrogen concentrations gives the monolayer ratio for exact strain balancing. Based on these estimations, hereafter, the monolayer ratio for the two layers of the superlattice is chosen to be $\sim 1:3$.

III. BAND STRUCTURE NEAR THE CENTER OF THE BRILLOUIN ZONE (Γ POINT)

A. Effects of strain on the band structure

In-plane strain on a lattice mismatched ternary $AB_{1-x}C_x$ epilayer grown on a thick substrate, as defined in Eq. (3), is given as

$$\varepsilon_{\parallel} = \frac{a_0 - a(x)}{a(x)}, \tag{8}$$

where a_0 is the lattice constant of the substrate and $a(x) = (1-x)a_{AB} + xa_{AC}$ is the lattice constant of the ternary $AB_{1-x}C_x$. For compressive strain, for example, for $InAs_{1-y}N_y$ lattice matched to InP, $a(y) > a_0$ therefore the in-plane strain is negative. On the other hand, it is positive for a tensile strain material, for example, for $GaAs_{1-x}N_x$ lattice matched to InP, where $a(x) < a_0$. Using Eqs. (3), (4), and (8) for a strained layer, the conduction band is shifted by[20]

$$\delta E_{CB} = a_c(2\varepsilon_{xx} + \varepsilon_{zz}) = 2a_c\left(1 - \frac{C_{12}}{C_{11}}\right)\varepsilon_{\parallel}. \tag{9}$$

Due to the sign and magnitude of the hydrostatic deformation potential a_c, the conduction band lowers for the tensile strain and moves up for the compressive strain in comparison to the unstrained position. The conduction bands are subjected only to the hydrostatic deformation potential.[21] Due to the valence-band component of hydrostatic deformation potential a_v, the center of gravity of the valence band of a strained epilayer shifts by an amount[20]

TABLE I. Physical quantitites related to strain and their effects on the bands.

Quantity	Compressive strain ($InAs_{1-y}N_y/InP$)	Tensile strain ($GaAs_{1-x}N_x/InP$)
In-plane strain, $\varepsilon_{\parallel}=\frac{a_0-a}{a}$	Negative	Positive
Perpendicular strain $\varepsilon_{zz}=\varepsilon_{\perp}=-\frac{2C_{12}}{C_{11}}\varepsilon_{\parallel}$	Positive	Negative
Conduction-band shift, $\delta E_{CB}=a_c(2\varepsilon_{xx}+\varepsilon_{zz})$	Positive	Negative
Valence-band shift due to the hydrostatic deformation potential, $-P=a_v(\varepsilon_{xx}+\varepsilon_{yy}+\varepsilon_{zz})$	Negative	Positive
$m_j=\pm 3/2$ hole shift due to the tetragonal deformation potential, $-Q=\frac{b}{2}(\varepsilon_{xx}+\varepsilon_{yy}-2\varepsilon_{zz})$	Positive	Negative
$m_j=\pm 1/2$ hole shift due to the tetragonal deformation potential, $\frac{(Q-\Delta)}{2}+\frac{1}{2}\sqrt{9Q^2+\Delta^2+2Q\Delta}$	Negative	Positive

$$-P=a_v(\varepsilon_{xx}+\varepsilon_{yy}+\varepsilon_{zz}). \tag{10}$$

On the other hand, the tetragonal deformation potential removes the degeneracy of the $m_j=\pm 3/2$ and $m_j=\pm 1/2$ valence subbands at $k=0$ and induces an energy shift of these bands in opposite directions. The analytical expressions for the magnitude of these shifts for $m_j=\pm 3/2$ and $m_j=\pm 1/2$ subbands is given by[20]

$$-Q=\frac{b}{2}(\varepsilon_{xx}+\varepsilon_{yy}-2\varepsilon_{zz}) \tag{11}$$

and

$$\frac{(Q-\Delta)}{2}+\frac{1}{2}\sqrt{9Q^2+\Delta^2+2Q\Delta}, \tag{12}$$

respectively. Here, Δ is the spin-orbit coupling term. Hence the net shift of the $m_j=\pm 3/2$ and $m_j=\pm 1/2$ hole bands with respect to the unstrained valence-band maxima is given as

$$\delta E_{|m_j=\pm 3/2\rangle}=-P-Q \tag{13}$$

and

$$\delta E_{|m_j=\pm 1/2\rangle}=-P+\frac{(Q-\Delta)}{2}+\frac{1}{2}\sqrt{9Q^2+\Delta^2+2Q\Delta}, \tag{14}$$

respectively. Total separation between the two valence subbands is then given as

$$\delta E=\delta E_{|m_j=\pm 1/2\rangle}-\delta E_{|m_j=\pm 3/2\rangle}$$
$$=\frac{(3Q-\Delta)}{2}+\frac{1}{2}\sqrt{9Q^2+\Delta^2+2Q\Delta}. \tag{15}$$

Table I summarizes the effect of the strain on the conduction and valence bands. Negative or positive in the second and third columns shows a decrease or increase of the energy of the band with respect to the fixed unstrained band maxima. Here it is worth noting that for a given layer the lattice constant will also depend on the change in the temperature. This consideration may be important for practical realizations since the growth temperatures for the semiconductors of interest (>450 °C) is generally different from the operating temperature. Since the thermal expansion coefficients of materials considered here are not the same, an additional thermoelastic strain may be generated in the system. As discussed by Freundlich *et al.*,[22] when the temperature of GaAs on InP is dropped from growth temperature (~650 °C) to the operating room temperature, the magnitude of the thermoelastic stress is ~1 kbar, which corresponds to the variation of the band gap in the order of 10 meV.

Material parameters used for the calculations are given in Table II. All of the parameters of the III-V-N, except the band gap, are determined by the linear extrapolation of the parameters for binaries.[23–26] Temperature dependence of the band gaps is determined by a Varshni-like formula[27] given as

$$E_g(T)=E_g(T=0)-\frac{\theta T^2}{T+\beta}, \tag{16}$$

where T is the absolute temperature, and θ and β are the experimentally fitted parameters given in Table II.

TABLE II. Material parameters used for the calculations.

Parameter	GaAs	InAs	GaN	InN
Lattice constant (Å)	5.653	6.0583	4.50	4.98
Energy band gap (eV) (0 K),	1.519	0.417		
θ (meV/K)	0.5405	0.276		
β (K)	204	93		
Thermal expansion, α (10^{-6} K^{-1})	5.6	4.6		
Δ_{SO}(meV)	341	390	17	0.006
m_e/m_0	0.067	0.026		
γ_1	6.98	20.0	2.67	3.72
γ_1	2.06	8.5	0.75	1.26
a_c (eV)	−7.17	−5.08	−2.2	−1.85
a_v (eV)	2	1.00	5.2	1.5
b (eV)	−1.66	−1.8	−2.2	−1.2
C_{11}(10^{11} dynes cm^{-2})	11.9[a]	8.329[a]	29.6[a]	18.7[b]
C_{12} (10^{11} dynes cm^{-2})	5.38[a]	4.526[a]	13.0[a]	12.5[b]

[a]Reference 25.
[b]Reference 26.

B. Evolution of the conduction band of strained layers of $GaAs_{1-x}N_x$ and $InAs_{1-y}N_y$

The band anticrossing (BAC) model was introduced by Shan *et al.*[28] to explain the two-level repulsion observed in the GaInNAs alloys.[29] Despite the simple physical nature, the model has been shown to describe the material properties of III-V-N very well.[30–33] It explains the pressure and concentration dependencies of the $GaAs_{1-x}N_x$ alloy by introducing a conduction-band splitting caused by the anticrossing interaction between the N-localized state and the conduction band of host III-V matrix. The new conduction subbands originated by such a splitting due to the N-induced perturbation are denoted as E_- and E_+ and are given as[28]

$$E_{\pm}(k) = \frac{1}{2}\left\{E_N + E_{III\text{-}V}(k) \pm \sqrt{[E_N - E_{III\text{-}V}(k)]^2 + 4xV_N^2}\right\}, \tag{17}$$

where E_N is the energy of the localized nitrogen state, $E_{III\text{-}V}(k)$ is the dispersion of the host crystal conduction band, V_N is the strength of the anticrossing interaction between the N-localized states and the conduction-band states of host matrix, and x is the nitrogen concentration. All the energies are relative to the valence-band maximum of the unperturbed host crystal. The BAC model with V_N=2.7 eV provides an excellent fit for the nitrogen concentration $x \leq 0.03$. With a larger x, there is some discrepancy between the experimental band gap and the BAC model.[34] Other than the pressure and compositional band-gap dependence, the BAC model was also used successfully to predict an increase in the electron effective mass in III-V-N alloys. It gives a simple analytic expression for the electron effective mass that can be directly extracted from Eq. (17) as

$$\frac{1}{m^*} = \frac{1}{\hbar^2}\left|\frac{\partial^2 E_-(k)}{\partial k^2}\right|_{k=0} = \frac{1}{2m_{III\text{-}V}}\left[1 - \frac{E_{III\text{-}V}(k) - E_N}{\sqrt{\{[E_{III\text{-}V}(k) - E_N]^2 + 4xV_N^2\}}}\right], \tag{18}$$

where $m_{III\text{-}V}$ is the electron effective mass in the host crystal in the absence of nitrogen. Note that, near k=0, $[E_{III\text{-}V}(k) - E_N]$ is a negative quantity. Equation (18) can be simplified to give

$$m^* = m_{III\text{-}V}\left[1 + \frac{xV_N^2}{(E_N - E_-)^2}\right]. \tag{19}$$

The model predicts that the effective mass will increase rapidly to about $0.1m_0$ until x=0.01 and then saturates to the value of about $0.11m_0$ for larger x. It is worth noting that, in practice, higher nitrogen concentrations have yielded effective masses in excess of $0.2m_0$ (e.g., see Ref. 34, and references therein).

C. Evolution of the valence band of strained layers of $GaAs_{1-x}N_x$ and $InAs_{1-y}N_y$

For the calculation of valence bands, we use the Luttinger-Kohn model based on a six-band $\boldsymbol{k}\cdot\boldsymbol{p}$ approximation[35,36] including the spin-orbit effects. We include the effects of strain using a formalism described by Bir and Pikus.[37] Since the coupling between conduction and valence bands is proportional to $\boldsymbol{k}$, for $\boldsymbol{k}\sim 0$ conduction band decouples with the valence band, favoring the six-band model. Recently, eight-band $\boldsymbol{k}\cdot\boldsymbol{p}$ model has also been used after modification to include the 2×2 interaction matrix for nitrogen and GaAs host material to produce 10×10 $\boldsymbol{k}\cdot\boldsymbol{p}$ model,[38–40] including the interaction of the conduction and valence bands.

The full 6×6 matrix can be block diagonalized into two 3×3 matrices, and in k_z direction is given as[41]

$$H = \begin{bmatrix} H_{11}(k_z) & 0 & 0 \\ 0 & H_{22}(k_z) & \Delta_1 \\ 0 & \Delta_1 & H_{33}(k_z) \end{bmatrix} \begin{matrix} |3/2, \pm 3/2\rangle \\ |3/2, \pm 1/2\rangle \\ |1/2, \pm 1/2\rangle \end{matrix}, \tag{20}$$

where

$$H_{11}(k_z) = \frac{\hbar^2}{2m_0}(2\gamma_2 - \gamma_1)k_z^2 - P - Q,$$

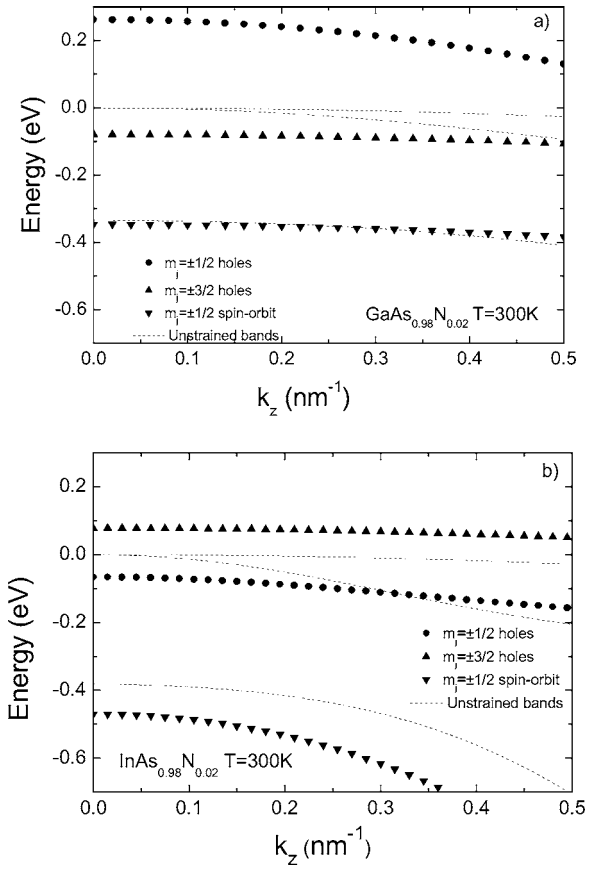

FIG. 4. Band structure of (a) bulk $GaAs_{0.98}N_{0.02}$ on InP (001) at 300 K for $k_x=k_y=0$. The $m_j=\pm 3/2$ hole band is moved down relative to the $m_j=\pm 1/2$ hole band, removing the degeneracy at k=0. (b) bulk $InAs_{0.98}N_{0.02}$ on InP (001) at 300 K for $k_x=k_y=0$. The $m_j=\pm 1/2$ hole band is moved down relative to the $m_j=\pm 3/2$ hole band. Unstrained structure is given by the dotted line.

$$H_{22}(k_z) = H_{11} - \frac{2}{3}\Delta,$$

$$H_{33}(k_z) = -\frac{1}{3}\Delta - \frac{\hbar^2}{2m_0}(2\gamma_1 + 4\gamma_2)k_z^2 - P + 2Q,$$

$$\Delta_1 = \frac{2}{3}\Delta, \tag{21}$$

and γ_1 and γ_2 are the Luttinger parameters for effective masses, m_0 is the electron mass, k_z is the wave vector along the z direction (along the direction of the growth), $\hbar$ is the Planck constant/2π. In the k_z direction, carriers corresponding to the $m_j = \pm 3/2$ band get decoupled from the rest of the bands, with the dispersion relation given as

$$E_{m_j=\pm 3/2} = H_{11} = \frac{\hbar^2}{2m_0}(2\gamma_2 - \gamma_1)k_z^2 - P - Q. \tag{22}$$

The remaining 2×2 matrix can be used to find the coupled dispersion relation for $m_j = \pm 1/2$ and spin-orbit states as

$$E_{so}^{m_j=\pm 1/2} = \frac{1}{2}\{[H_{33}(k_z) + H_{22}(k_z)]\} \pm \frac{1}{2}[\sqrt{[H_{33}(k_z) + H_{22}(k_z)]^2 - 4\{H_{33}(k_z) \times H_{22}(k_z) - (\sqrt{2}/3\Delta)^2\}}], \tag{23}$$

where the $m_j = \pm 1/2$ dispersion corresponds to the + sign and the spin-orbit dispersion to the − sign in the right-hand side of the equation.

Figures 4(a) and 4(b) show the valence-band structure of the bulk $GaAs_{0.98}N_{0.02}$ and $InAs_{0.98}N_{0.02}$ layer strained on InP(001). The band energy is plotted as a function of k_z ($k_x = k_y = 0$). Degeneracy between $m_j = \pm 3/2$ and $m_j = \pm 1/2$ hole bands at the zone center has been removed due to the strain effects, as discussed earlier in Sec. III A. For $GaAs_{0.98}N_{0.02}$, being tensilely strained, the $m_j = \pm 3/2$ band is moved lower than $m_j = \pm 1/2$, as can be seen from the definitions in Table I, an effect which is opposite in the compressively strained $InAs_{1-x}N_x$ on InP(001). Dotted curves in figures show the band structure for the unstrained bulk layer.

IV. BAND-STRUCTURE CALCULATIONS OF A SUPERLATTICE: TRANSFER-MATRIX ALGORITHM

A. Transfer-matrix method

For a fixed energy and fixed in-plane wave vectors k_x and k_y, we can construct the total envelope function of a superlattice as a linear combination of the eigenvectors of the corresponding Hamiltonian. For each region j, the full envelope function has the general shape

$$\Psi(z) = \sum_q a_q^j \boldsymbol{F}_q^j e^{ik_{zj}^q(z-l_j)} + \sum_q b_q^j \boldsymbol{F}_q^j e^{-ik_{zj}^q(z-l_j)}, \tag{24}$$

where the sum is over all the bands q (CB, VB), a_q^j and b_q^j are complex constants, $\boldsymbol{F}_q^j$ are eigenvector matrices, and l_j defines the distance of the jth interface from the origin.

Boundary conditions at each interface are[42]

$$\Psi^j\big|_{z=l_j} = \Psi^{j+1}\big|_{z=l_{j+1}} \quad \text{and}$$

$$\frac{1}{m_j}\frac{\partial \Psi^j}{\partial z}\bigg|_{z=l_j} = \frac{1}{m_{j+1}}\frac{\partial \Psi^{j+1}}{\partial z}\bigg|_{z=l_{j+1}}. \tag{25}$$

Here, m_j is the effective mass in the jth layer. For $k_x = k_y = 0$, the $m_j = \pm 3/2$ hole band gets decoupled from the rest of the bands, and the transfer matrix can be found applying the above two boundary conditions to relate constants a and b of the jth and $(j+1)$th layers, and is given as

$$\begin{pmatrix} a^j \\ b^j \end{pmatrix} = M_{j(j+1)} \begin{pmatrix} a^{j+1} \\ b^{j+1} \end{pmatrix}, \tag{26}$$

where

$$M_{j(j+1)} = \begin{pmatrix} 1 + \frac{m_j k_{j+1}}{m_{j+1} k_j} & 1 - \frac{m_j k_{j+1}}{m_{j+1} k_j} \\ 1 - \frac{m_j k_{j+1}}{m_{j+1} k_j} & 1 + \frac{m_j k_{j+1}}{m_{j+1} k_j} \end{pmatrix} \times \begin{bmatrix} e^{-ik_{j+1}L_{j+1}} & 0 \\ 0 & e^{ik_{j+1}L_{j+1}} \end{bmatrix}. \tag{27}$$

Here, L_j is the thickness of the jth layer. For a large number of layers, the total transfer matrix can be written as the product of transfer matrices across each layer,

$$\begin{pmatrix} a^1 \\ b^1 \end{pmatrix} = M_{total} \begin{pmatrix} a^N \\ b^N \end{pmatrix},$$

$$M_{total} = \begin{pmatrix} m_{11} & m_{12} \\ m_{21} & m_{22} \end{pmatrix} = M_{12} M_{23} M_{34} \cdots. \tag{28}$$

We now require $a^1 = b^N = 0$ for decaying solutions in the first and last barriers, the width of which is assumed to be large enough for this condition to hold. To satisfy this condition, the element m_{11} goes to zero and hence the solution of the equation $m_{11}(E) = 0$ provides the energy states of the corresponding carriers in $m_j = \pm 3/2$ hole states. The same process can be repeated for $m_j = \pm 1/2$ states also, but due to the

interaction with spin-orbit split-off states we have to deal with a 4×4 transfer matrix, with added numerical complexity.

B. Miniband energies in the superlattice

Subband energy calculations of the $(GaAs_{1-x}N_x)_m/(InAs_{1-y}N_y)_n$ superlattice is done under the envelope function approximation, using the transfer-matrix method as described earlier and demonstrated in previous works.[43,44] Due to the high probability of the wave-function penetration through the thin barriers separating the wells, Pauli's principle suggests the formation of separate energy level for each well for a given carrier type. Hence in the presence of large number of wells in a given superlattice, crowded separate energy levels form the minibands for different types of carriers in different bands, *viz.*, conduction, $m_j=\pm1/2$, and $m_j=\pm3/2$ bands. Increasing the number of wells increases the width of the minibands with small change in the miniband edge. Increase in the well thickness moves the miniband edge closer to the bulk band edge, but due to the critical thickness limits of the strained layer, as discussed in Sec. II, there is not much choice for such a variation. Variation of nitrogen concentration, on the other hand, changes the conduction miniband edge significantly, with small strain related changes in the valence miniband edge. The gap between the band-edge extrema of the conduction miniband and the valence miniband determines the electrical and optical properties of the structure. The energy gap between the first $m_j=\pm1/2$ miniband edge to the first electron miniband edge $(E_{1/2})$ and the one between the $m_j=\pm3/2$ miniband edge to the first electron miniband edge $(E_{3/2})$ correspond to the onset of absorption and emission energies of the structure, as shown in Fig. 5 for $x=y=0.01$. In Fig. 5, the band edge of the InAsN valence band is assumed as the reference zero (refer to the Fig. 5 caption for more details). For a given thickness of the $GaAs_{1-x}N_x$ layer (3 monolayers), the thickness of the $InAs_{1-y}N_y$ layer is chosen to strain balance the superlattice structure on the InP substrate. As the miniband edges of the valence and conduction bands changes with the nitrogen incorporation, due to the anomalous band-gap reduction of the bulk $GaAs_{1-x}N_x$ and $InAs_{1-y}N_y$, the effective band gap of the structure varies. Figure 6 shows the evolution of $E_{3/2}$ as a function of the nitrogen concentrations at 300 K. This graph also shows the variation in the nature of the curves for different amounts of nitrogen concentration in InAs(N) in proportion to the nitrogen concentration in GaAs(N). For the top curve (dash dot), the nitrogen concentration is zero in InAs and is the upper limit for the effective band gap of the superlattice structure for given nitrogen concentration in GaAsN. With the addition of nitrogen in InAs, its band gap reduces and it also reduces the effective band gap of the superlattice for a given nitrogen concentration in GaAs(N). As an example, this trend is shown for two typical nitrogen concentrations in $InAs_{1-y}N_y$, $y=x/2$, and $y=x$, as shown by the dashed and solid curves, respectively. Hence the variation of nitrogen concentration can be taken as an added parameter to control the effective features of the superlattice structure. It can be seen that by varying the nitrogen concentration the emission and absorption energies of the structure can be tuned from ~0.64 to ~0.35 eV for $x,y\leq0.05$, at $T=300$ K, showing the potential of these heterostructures for attaining operating wavelengths beyond 3 μm on InP.

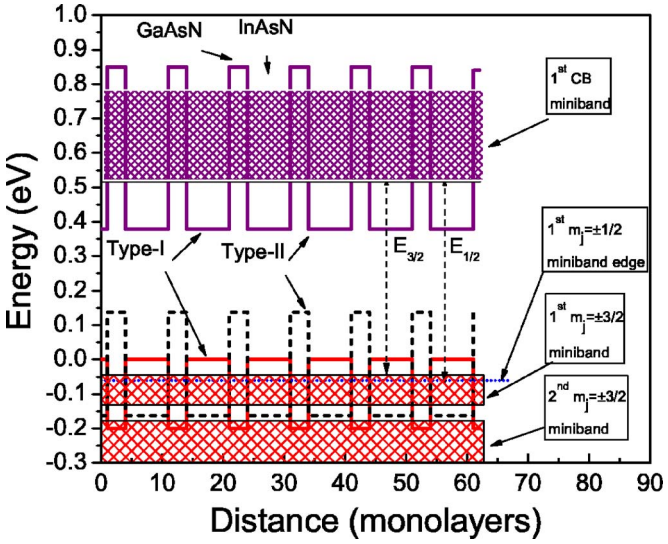

FIG. 5. (Color online) Calculated diagram of the type-I (conduction band and valence bands as solid lines) and type-II (valence band as dashed line) band alignments for 20 period $GaAs_{0.99}N_{0.01}$(3 MLs)/$InAs_{0.99}N_{0.01}$(7 MLs) superlattice system. Also shown is the effective band gap as a separation of miniband edges in conduction and valence subbands. For clarity purposes, only the edge of the $m_j=\pm1/2$ miniband is shown as a small dotted horizontal line in the valence band.

One of the alternatives to the strain-balanced superlattice $(GaAs_{1-x}N_x)_m/(InAs_{1-y}N_y)_n$ is the quaternary alloy

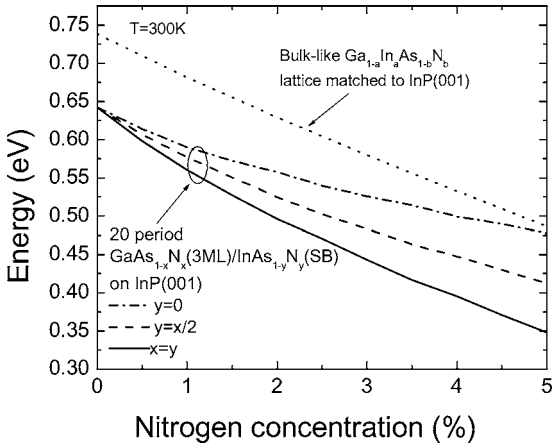

FIG. 6. Evolution of energy gaps $E_{3/2}$, between the $m_j=\pm3/2$ holes and the electron minibands of a 20 period $GaAs_{1-x}N_x$(3 MLs)/$InAs_{1-y}N_y$ SL as a function of the nitrogen concentration at 300 K for $y=x/2$, $y=x$, and $y=0$. Note that for each different nitrogen data point the thickness of the $InAs_{1-x}N_x$ sublayers (4–9 MLs) is adjusted to satisfy the lattice matching condition of the SL to InP (001). Also shown is the band-gap variation of the InGaAsN quaternary alloy with nitrogen concentration, when the lattice is matched to InP.

$In_aGa_{1-a}As_{1-b}N_b$, where $a=n/(m+n)$ and $b=(mx+ny)/(m+n)$. This alloy can be grown on GaAs or InP substrates, but has its own limitations. The novel quaternary alloy allows the tuning of the band gap from 1.42 eV to below 1 eV on GaAs substrate. Lattice matched $In_aGa_{1-a}As_{1-b}N_b$ on InP has recently been investigated for the potential use in the mid-infrared device applications,[45] with a potential of giving a band gap as low as 0.6 eV.[28,30,38,46,47] Yet access to lower band gaps is highly desirable for many mid-IR device applications like mid-IR lasers or thermophotovoltaic converters.[48] To lower the band gaps further, either the alloy has to be strained, which may produce defect related problems causing a short life span of the devices or the need to introduce a high content of indium which again further complicates the growth procedure and restricts the amount of nitrogen content.[49–51] Furthermore, although the increase of the nitrogen incorporation is a possibility,[52] alloys with nitrogen beyond 4–5 % exhibit poor material quality, making them inadequate for many optoelectronic applications. Under the BAC model approximation the band gap of InGaAsN lattice matched on InP is shown in Fig. 6. It is worth noting that the "ordered alloys effect"[53] associated with the use of the proposed superlattice allows a significant band-gap reduction (about 100 meV) in comparison to that of a quaternary (bulklike) InGaAsN of similar average concentration.

V. ABSORPTION COEFFICIENTS

Optical absorption in a semiconductor material is one of the very important physical phenomena to be considered for the application in many optoelectronic devices. The parameter that characterizes the optical absorption is called the absorption coefficient and is defined as the ratio of the number of photons absorbed per unit volume per second to the number of photons injected per unit area per second. Hence the absorption coefficient gives the fraction of photons absorbed per unit distance and is denoted by α (cm^{-1}). Absorption coefficients of the bulk semiconductors and quantum wells have been studied intensively in many texts [for example, Chap. 13, of Ref. 20 and references therein].

The absorption coefficient α in the crystal for a bulk semiconductor is given as[20]

$$\alpha(\hbar\omega) = 2A_0 \sum_n |\phi_n(0)|^2 \delta(\hbar\omega - E_g - E_n), \tag{29}$$

where $A_0=\frac{\pi e^2|\hat{i}\cdot\boldsymbol{p}_{cv}|^2}{n_r c\varepsilon_0 m_0^2\omega}$, $\hat{i}$ is the unit vector along the direction of the propagation of the incoming photon, $\boldsymbol{p}_{cv}$ is the transition-matrix element between the conduction and valence bands, e is an electronic charge, n_r is the refractive index, c is the velocity of the electromagnetic wave in a vacuum, ε_0 is the permittivity of the vacuum, m_0 is the electron mass, ω is the angular frequency of the incoming electromagnetic wave, $\hbar$ is the Planck's constant/2π, $R_y=\frac{1}{(4\pi\varepsilon_s)^2}\frac{\mu_r e^4}{2\hbar^2}$, μ_r is the reduced effective mass of holes and electrons and is given as $\frac{1}{\mu_r}=\frac{1}{m_e}+\frac{1}{m_h}$, $\varepsilon_s=K\varepsilon_0$, K is a dielectric constant, $\phi_n(0)$ is a normalized wave function for both bound and continuum states and is given as

$$\phi_n(0)\Big|_{bound} = \frac{1}{\pi a_{00}^3 n^3}, \tag{30}$$

and

$$\phi_E(0)\Big|_{continuum} = \frac{e^{\pi/\sqrt{E/R_y}}}{4\pi R_y a_{00}^3 \sinh(\pi/\sqrt{E/R_y})}, \tag{31}$$

respectively. Here, the excitonic Bohr radius $a_{00}=\frac{4\pi\varepsilon_s\hbar^2}{e^2\mu_r}$. With inclusion of this, the total absorption (also called Elliott formula) due to both bound and continuum states in bulk semiconductor can be given as (for example, Ref. 20)

$$\alpha(\hbar\omega) = \frac{A_0}{2\pi^2 R_y a_{00}^3}\left[4\sum_{n=1}^{\infty}\frac{\Gamma/n^3}{(\Xi+1/n^2)+\Gamma^2} + \frac{\pi e^{\pi/\sqrt{\Xi}}}{\sinh(\pi/\sqrt{\Xi})}\right], \tag{32}$$

where $\Xi=\frac{\hbar\omega-E_g}{R_y}$, and Γ is the Lorenzian width corresponding to the phonon broadening.

For the superlattice structure discussed in Sec. IV, we will use an anisotropic medium approach, in which the absorption coefficient of the bulk material is modified to take care of the anisotropy introduced by the presence of the superlattice periodicity. As discussed in Sec. IV, due to the penetration of the carrier wave function into the adjacent wells separated by thin barriers in a superlattice, the coupling between the two neighboring wells is very large to allow for the hybridization of the original discrete energy levels of isolated wells into minibands. The electron and hole tunneling through the minibands leads to the motion in the growth direction, which is characterized by the effective masses modified by the superlattice potential. The superlattice is then characterized by a three-dimensional effective medium with different in-plane and growth-direction effective masses.

The superlattice absorption coefficient then can be assumed as a deviation from a bulk absorption coefficient by considering the anisotropy introduced in the reduced effective masses of the carriers in the plane of the layers (in-plane reduced effective mass $\mu_\parallel$) and perpendicular to the plane of layers (growth direction or transverse reduced effective mass $\mu_\perp$), respectively. The ratio of these two masses can be defined as an anisotropy parameter,

$$\gamma = \mu_\parallel/\mu_\perp. \tag{33}$$

This parameter modifies the absorption coefficient as suggested in Ref. 54, and is given as

$$\alpha(\hbar\omega,\gamma) = \frac{A_0}{2\pi^2 R_y'(\gamma) a_{00}'(\gamma)^3}\left(\frac{2}{1+\gamma}\right)^2 \times\left[4\sum_{n=1}^{\infty}\frac{\Gamma/n^3}{[\varepsilon'(\gamma)+1/n^2]+\Gamma^2} + \frac{\pi e^{\pi/\sqrt{\Xi'(\gamma)}}}{\sinh[\pi/\sqrt{\Xi'(\gamma)}]}\right], \tag{34}$$

where

$$\Xi'(\gamma) = \frac{\hbar\omega - E_g}{R_y'(\gamma)}, \quad a_{00}'(\gamma) = \frac{4\pi\varepsilon_s\hbar^2}{e^2 m_\parallel},$$

$$R_y'(\gamma) = \frac{1}{(4\pi\varepsilon_s)^2}\frac{m_\parallel e^4}{2\hbar^2}, \quad m_\parallel = \frac{2\mu_\parallel}{1+\gamma}.$$

The in-plane and transverse reduced effective mass can be calculated as

$$\frac{1}{\mu_\parallel} = \frac{1}{m_{e_\parallel}} + \frac{1}{m_{h_\parallel}}, \quad \frac{1}{\mu_\perp} = \frac{1}{m_{e_\perp}} + \frac{1}{m_{h_\perp}}. \tag{35}$$

The in-plane effective mass $m_\parallel$ is assumed to be the average of effective masses of two different layers w and b of thickness L_w and L_b, respectively, in superlattice

$$m_{i_\parallel} = \frac{m_i^w L_w + m_i^b L_b}{L_w + L_b} \quad \text{with } i = e, \quad lh, \text{ or } hh. \tag{36}$$

As a first approximation, transverse effective mass $m_\perp$ can be obtained from

$$\frac{1}{m_\perp} = \left.\frac{1}{\hbar^2}\frac{d^2E}{dq^2}\right|_{q=0} \tag{37}$$

where the energy E is extracted from a dispersion relation for a superlattice[42]

$$\cos(qd) = \cos(k_w L_w)\cosh(k_b L_b) - \frac{1}{2}\left(\xi - \frac{1}{\xi}\right)\sinh(k_b L_b)\sin(k_w L_w), \tag{38}$$

where $k_w = \sqrt{\frac{2m_w E}{\hbar^2}}$, $k_b = \sqrt{\frac{2m_b(V-E)}{\hbar^2}}$ for $E < V$ and $\xi = \frac{k_w m_b}{k_b m_w}$.

Using Eqs. (37) and (38), we may derive the transverse effective mass as

$$\begin{aligned} m_\perp = -\frac{\hbar^2}{d^2}[&-\cos(L_w k_w)\sinh(L_b k_b)L_b B \\ &- \sin(L_w k_w)\cosh(L_b k_b)L_w A] \\ &- \frac{\hbar^2}{d^2}\left[-\frac{1}{2}\frac{1}{\xi^2}\frac{m_b}{m_w}\left(\frac{A}{k_b} + \frac{Bk_w}{k_b^2}\right)\sinh(L_b k_b)\sin(L_w k_w)\right] \\ &- \frac{\hbar^2}{d^2}\left[-\frac{1}{2}\left\{\xi - \frac{1}{\xi}\right\}\{-\cosh(L_b k_b)\sin(L_w k_w)L_b B \right. \\ &\left. + \sinh(L_b k_b)\cos(L_w k_w)L_w A\}\right], \end{aligned} \tag{39}$$

where $A = \sqrt{\frac{m_w}{2\hbar^2 E}}$, $B = \sqrt{\frac{m_b}{2\hbar^2(V-E)}}$ and $d = L_w + L_b$.

Since the dielectric constant of GaAs(N) and InAs(N) are not very different from each other,[25] the ratio of the in-plane and transverse dielectric constants for a superlattice structure is ~1. Hence the dielectric constant of the superlattice is taken as the weighted average for two layers of superlattice as

$$\varepsilon^2 = \frac{\varepsilon_w L_w + \varepsilon_b L_b}{L_w/\varepsilon_w + L_b/\varepsilon_b}. \tag{40}$$

For $\gamma = 1$, Eq. (34) becomes similar to Eq. (32) and the condition corresponds to the one of no anisotropy or the bulk material absorption coefficient.

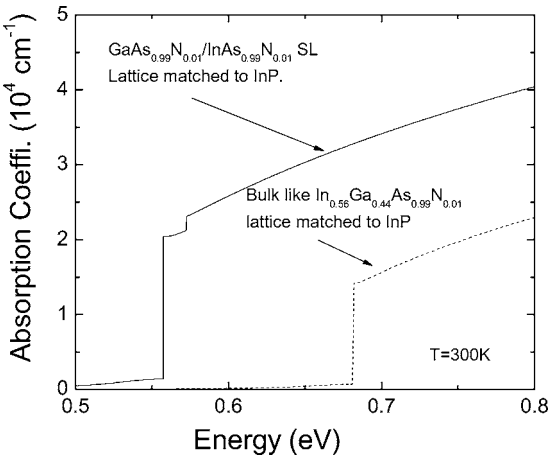

FIG. 7. Absorption coefficient of 20 period $GaAs_{0.99}N_{0.01}$(3 MLs)/$InAs_{0.99}N_{0.01}$ (7 MLs) superlattice strain-balanced to InP(001). For comparison purpose the absorption coefficient of the bulklike $In_{0.56}Ga_{0.44}As_{0.99}N_{0.01}$, lattice matched to InP, is also given.

In the presence of the alternate layers of $GaAs_{1-x}N_x$ and $InAs_{1-y}N_y$, the value of γ is always less than unity and it decreases with thicker barriers (or more anisotropy). Using the formalism derived from Eqs. (29)–(40), the room-temperature (300 K) absorption coefficients of 20 period $GaAs_{0.99}N_{0.01}/InAs_{0.99}N_{0.01}$ superlattice strain balanced to InP(001) is shown in Fig. 7 and compared with that of the bulklike $In_{0.56}Ga_{0.44}As_{0.99}N_{0.01}$ layer with the same average concentration. The In concentration in the bulklike layer is chosen to make it lattice matched to InP. A lower band-gap threshold of the absorption by the superlattice structure can be seen in comparison to that of the bulklike material for given nitrogen concentration, when both are lattice matched to InP. In addition to the absorption of lower energy photons, the magnitude of the absorption is also enhanced by the factor of ~1.5, which, in part is associated with the significantly higher effective masses of the carriers in the superlattice structure. The heavier effective-mass contribution comes from the presence of the nitrogen related effects and the anisotropy produced by the superlattice potential in the direction of the growth. The contribution of the photon absorption between the higher-order minibands in the valence and conduction bands of the superlattice structure would only be seen in the energy range of ≥0.8 eV and hence is neglected in the study because it falls in the energy range beyond our interest.

Figure 8 shows the variation of the absorption coefficient of $GaAs_{0.99}N_{0.01}/InAs_{0.99}N_{0.01}$ superlattice structure with temperature, excitonic effects are pronounced below ~50 K, due to the stronger Coulombic attraction between the holes and electrons because of reduced thermalization (or phonon broadening). At higher temperatures, the excitonic absorption vanishes gradually. The variation of the effective band gap of the superlattice structures, used to demonstrate the absorption coefficients, with the temperature is based on the Varshni-like formula given in Eq. (16). Figure 9 shows the variation of the absorption coefficients of the $GaAs_{0.99}N_{0.01}/InAs_{0.99}N_{0.01}$ superlattice structure, with re-

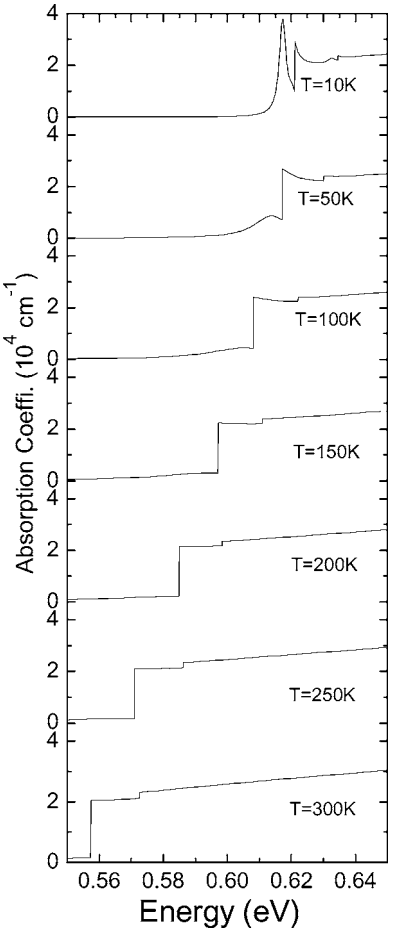

FIG. 8. Variation of the absorption coefficient of 20 period $GaAs_{0.99}N_{0.01}$(3 MLs)/$InAs_{0.99}N_{0.01}$ (7 MLs) superlattice strain-balanced to InP(001) for different temperatures.

spect to the nitrogen concentration at 10 K. It can be seen that the lower energy photons can be absorbed, with relatively higher magnitude of the absorption coefficients, as the nitrogen concentration increases. This can be understood by the fact that the band gap of the superlattice structure is

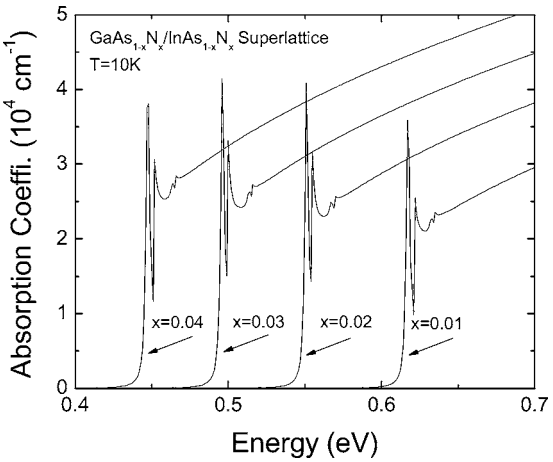

FIG. 9. Variation of the absorption coefficient of 20 period $GaAs_{1-x}N_x$(3 MLs)/$InAs_{1-x}N_x$ (7 MLs) superlattice strain-balanced to InP(001) for different nitrogen concentrations at 10 K.

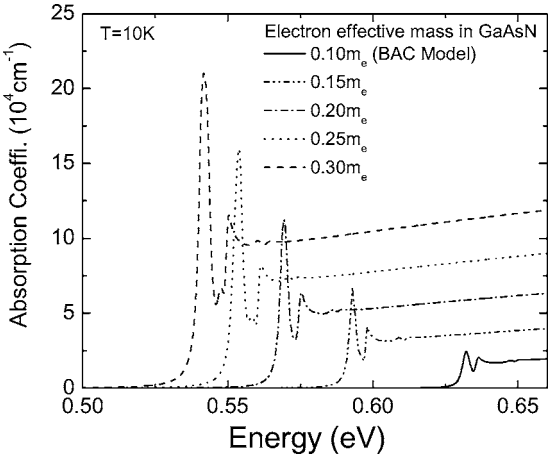

FIG. 10. Variation of the absorption coefficient of 20 period $GaAs_{0.99}N_{0.01}$(3 MLs)/$InAs_{0.99}N_{0.01}$ (7 MLs) superlattice strain-balanced to InP(001) for different electron effective mass.

reduced along with the increase in the effective mass of the carriers, as the nitrogen concentration increases. The behavior of the effective mass near the band edge of dilute nitrides is not understood fully yet, but there is some indication that it reaches the maximum for a certain value of nitrogen concentration.[55–57] The effect of the effective mass on the absorption coefficient is depicted in Fig. 10 for varying effective masses from $0.1m_e$ to $0.3m_e$. An increase in effective mass produces two effects: first it reduces the effective miniband edges, reducing the effective band gap of the superlattice structure, and second, it increases the magnitude of the absorption coefficient. Note, if the effective mass remains constant at a specific value (say $0.1m_e$), for any higher values of nitrogen the absorption coefficient would shift to the lower energies due to the lower band gaps produced by nitrogen effects only. It should also be noted that in this calculation the contribution of intersubband absorption, which may be important for some devices considering the free-carrier absorption or far-infrared absorption, is neglected. The simplicity of the analytical expression for the absorption coefficients including the excitonic effect and previously shown good quantitative agreement with the experimental results[54] makes this approach an ideal methodology for the quantitative evaluation of the coefficients.

VI. CONCLUSIONS

We have investigated the electronic properties of the conduction band and valence band of the strained $GaAs_{1-x}N_x$ and $InAs_{1-y}N_y$ on InP(001) for $k_x=k_y=0$. The ratio $m:n$ of the monolayer thicknesses of individual layers of $(GaAs_{1-x}N_x)_m$ and $(InAs_{1-x}N_x)_n$ needed to create a strain-balanced superlattice on InP(001) is determined by minimizing the total energy of the stack. For most of the calculations, the appropriate ratio is found to be $\sim 1:3$ with little or no residual strain on InP. A study of the effective band gap between the conduction and valence miniband edges of $(GaAs_{1-x}N_x)_m/(GaAs_{1-y}N_y)_n$ short period strain balanced superlattices is performed for different combinations of x and

y. The results predict the possibility of tuning photons absorption and emission wavelengths well beyond the 3-μm mark at 300 K, while maintaining the entire structure lattice matched to InP.

The optical-absorption coefficient of the superlattice structure is also determined as a function of nitrogen concentration, effective mass, and temperature, using the anisotropic medium approach, and compared with a bulklike InGaAsN. For a given nitrogen concentration and temperature, an absorption of lower energy photons with a magnitude $\sim$1.5 higher in comparison to that of the counterpart InGaAsN is found. At lower temperature ($<$50 K), the band edge of the structure was less pronounced due to the presence of strong excitonic contributions.

ACKNOWLEDGMENTS

This work was partially supported by the State of Texas Higher Education Coordinating Board Advanced Technology Grants No. 003652-0126-2001 and 003652-0316-2001 and NASA Grant No. NNC04GB53N.

*Corresponding author. Email address: afreundlich@uh.edu

[1] W. O. Groves, A. H. Herzog, and M. G. Craford, Appl. Phys. Lett. **19**, 184 (1971).
[2] M. Weyers, M. Sato, and H. Ando, Jpn. J. Appl. Phys., Part 2 **31**, L853 (1992); J. N. Baillargeon, K. Y. Cheng, G. E. Hofler, P. J. Pearah, and K. C. Hsieh, Appl. Phys. Lett. **60**, 2540 (1992).
[3] M. Kondow, K. Uomi, A. Niwa, T. Kitatani, S. Watahiki, and Y. Yazawa, Jpn. J. Appl. Phys., Part 2 **35**, 1273 (1996).
[4] S. R. Kurtz, A. A. Allerman, E. D. Jones, J. M. Gee, J. J. Banas, and B. E. Hammons, Appl. Phys. Lett. **74**, 729 (1999).
[5] A. Wagner, C. Ellmers, F. Hohnsdorf, J. Koch, C. Agert, S. Leu, M. Hofmann, W. Stolz, and W. W. Ruhle, Appl. Phys. Lett. **76**, 271 (2000).
[6] E.-M. Pavelescu, C. S. Peng, T. Jouhti, J. Konttinen, W. Li, M. Pessa, M. Dumitrescu, and S. Spanulescu, Appl. Phys. Lett. **80**, 3054 (2002).
[7] W. Li, T. Jouhti, C. S. Peng, J. Konttinen, P. Laukkanen, E.-M. Pavelescu, M. Dumitrescu, and M. Pessa, Appl. Phys. Lett. **79**, 3386 (2001).
[8] A. H. Bensaoula, A. Freundlich, A. Bensaoula, V. Rossignol, and A. Ponchet, J. Vac. Sci. Technol. B **12**, 1110 (1994).
[9] M. C. Tamargo, R. Hull, L. H. Greene, J. R. Hayes, and A. Y. Cho, Appl. Phys. Lett. **46**, 569 (1985).
[10] G. C. Osbourn, J. Appl. Phys. **53**, 1586 (1982).
[11] R. Hull, J. C. Bean, F. Cerdeira, A. T. Fiory, and J. M. Gibson, Appl. Phys. Lett. **48**, 56 (1986).
[12] J. W. Matthew and A. E. Blakeslee, J. Cryst. Growth **27**, 118 (1974).
[13] R. People and J. C. Bean, Appl. Phys. Lett. **47**, 322 (1985).
[14] J. F. Nye, *Physical Properties of Crystals* (Clarendon, Oxford, 1986), Chap. 8.
[15] N. J. Ekins-Daukes, K. Kawaguchi, and J. Zhang, Cryst. Growth Des. **2**, 287 (2002).
[16] L. Bhusal, A. Alemu, and A. Freundlich, Phys. Rev. B **74**, 199901 (2006).
[17] J. H. Vander Merwe, J. Appl. Phys. **34**, 123 (1962).
[18] J. P. Matthews and A. E. Blakeslee, J. Cryst. Growth **27**, 118 (1974).
[19] G. L. Price, Phys. Rev. Lett. **66**, 469 (1991).
[20] S. L. Chuang, in *Physics of Optoelectronic Devices* (Wiley, New York, 1995).
[21] C. G. Van de Walle, Phys. Rev. B **39**, 1871 (1981).
[22] A. Freundlich, J. C. Grenet, and G. Neu, Appl. Phys. Lett. **55**, 1558 (1989).
[23] I. Vurgaftman, J. R. Meyer, and L. R. Ram-Mohan, J. Appl. Phys. **89**, 5815 (2001).
[24] D. K. Shih, H. H. Lin, L. W. Sung, T. Y. Chu, and T. R. Yang, Jpn. J. Appl. Phys., Part 1 **42**, 375 (2003).
[25] O. Madelung, *Data in Science and Technology Series: Semiconductors: Group IV Elements and IIIV Compounds* (Springer-Verlag, Berlin, New York, 1991).
[26] A. F. Wright, J. Appl. Phys. **82**, 2833 (1997).
[27] Y. P. Varshni, Physica (Amsterdam) **34**, 149 (1967).
[28] W. Shan, W. Walukiewicz, J. W. AgerIII, E. E. Haller, J. F. Geisz, D. J. Friedman, J. M. Olson, and S R. Kurtz, Phys. Rev. Lett. **82**, 1221 (1999).
[29] J. D. Perkins, A. Mascarenhas, Y. Zhang, J. F. Geisz, D. J. Friedman, J. M. Olson, and S. R. Kurtz, Phys. Rev. Lett. **82**, 3312 (1999).
[30] K. M. Yu, W. Walukiewicz, W. Shan, J. W. AgerIII, J. Wu, E. E. Haller, J. F. Geisz, D. J. Friedman, and J. M. Olson, Phys. Rev. B **61**, R13337 (2000).
[31] J. Wu, W. Shan, W. Walukiewicz, K. M. Yu, J. W. AgerIII, E. E. Haller, H. P. Xin, and C. W. Tu, Phys. Rev. B **64**, 085320 (2001).
[32] M. Hofmann, A. Wagner, C. Ellmers, C. Schlichenmeier, S. Schäfer, F. Höhnsdorf, J. Koch, W. Stolz, S. W. Koch, W. W. Rühle, J. Hader, J. V. Moloney, E. P. O'Reilly, B. Borchert, A. Yu. Egorov, and H. Riechert, Appl. Phys. Lett. **78**, 3009 (2001).
[33] C. Skierbiszewski, S. P. Lepkowski, P. Perlin, T. Suski, W. Jantsch, and J. Geisz, Physica E (Amsterdam) **13**, 1078 (2002).
[34] J. A. H. Coaquira, L. Bhusal, W. Zhu, A. Fotkatzikis, M. A. Pinault, A. P. Litvinchuk, and A. Freundlich, in *Progress in Compound Semiconductor Materials IV—Electronic and Optoelectronic Applications*, edited by G. J. Brown, R. M. Biefeld, C. Gmachl, M. O. Manasreh, and K. Unterrainer, MRS Symposia Proceedings No. 829 (Materials Research Society, Pittsburgh, 2005), p. B11.3.
[35] E. O. Kane, in *Physics of III-V Compounds*, edited by R. K. Willardson and A. C. Beer, *Semiconductors and Semimetals* (Academic, New York, 1966), Vol. I, p. 75.
[36] E. O. Kane, in *Handbook on Semiconductors*, edited by T. S. Moss (North-Holland, Amsterdam, 1982), Vol. 1, Chap. 4A, pp. 193–217.
[37] G. L. Bir and G. E. Pikus, in *Symmetry and Strain-Induced Effects in Semiconductors* (Wiley, New York, 1974).
[38] S. A. Choulis, T. J. C. Hosea, S. Tomic, M. Kamal-Saadi, A. R. Adams, E. P. O'Reilly, B. A. Weinstein, and P. J. Klar, Phys.

Rev. B **66**, 165321 (2002).
[39] S. Tomic, E. P. Oreilly, R. Fehse, S. J. Sweeney, A. R. Adams, A. D. Andreev, S. A. Choulis, T. J. C. Hosea, and H. Riechert, IEEE J. Sel. Top. Quantum Electron. **9**, 1228 (2003).
[40] S. Tomic, E. P. O'Reilly, P. J. Klar, H. Gruning, W. Heimbrodt, W. M. Chen, and I. A. Buyanova, Phys. Rev. B **69**, 245305 (2004).
[41] S. H. Park and S. L. Chuang, J. Appl. Phys. **87**, 353 (2000).
[42] G. Bastard, *Wave Mechanics Applied to Semiconductor Heterostructures* (Halstead, New York, 1988).
[43] L. Bhusal, A. Alemu, and A. Freundlich, Phys. Rev. B **72**, 073309 (2005).
[44] L. Bhusal, A. Alemu, and A. Freundlich, Nanotechnology **15**, S245 (2004).
[45] K. Kohler, J. Wagner, P. Ganser, D. Serries, T. Geppert, M. Maier, and L. Kirste, J. Phys.: Condens. Matter **16**, S2995 (2004).
[46] M. R. Ghokale, J. Wei, H. Wang, and S. R. Forrest, Appl. Phys. Lett. **74**, 1287 (1999).
[47] P. Perlin, S. G. Subramanya, D. E. Mars, J. Kruger, N. A. Shapiro, H. Siegle, and E. R. Weber, Appl. Phys. Lett. **73**, 3703 (1998).
[48] L. Bhusal, A. Alemu, and A. Freundlich, *Proceedings of the 31st IEEE Photovoltaic Specialist Conference*, Orlando, FL, 2005, p. 133.
[49] D. J. Friedman, J. F. Geisz, S. R. Kurtz, J. M. Olson, and R. Reedy, J. Cryst. Growth **195**, 438 (1998).
[50] J. C. Harmand, G. Ungaro, L. Largeau, and G. Le Roux, Appl. Phys. Lett. **77**, 2482 (2000).
[51] S. B. Zhang and A. Zunger, Appl. Phys. Lett. **71**, 677 (1997).
[52] M.-A. Pinault, A. Freundlich, J. A. H. Coaquira, and A. Fotkatzikis, J. Appl. Phys. **98**, 023522 (2005).
[53] S. H. Wei and A. Zunger, Appl. Phys. Lett. **56**, 731 (1990).
[54] M. F. Pereira, Phys. Rev. B **52**, 1978 (1995).
[55] N. Shtinkov, P. Desjardins, and R. A. Masut, Phys. Rev. B **67**, 081202(R) (2003).
[56] A. Lindsay and E. P. O'Reilly, Solid State Commun. **112**, 443 (1999).
[57] C. Skierbiszewski, P. Pfeffer, and J. Łusakowski, Phys. Rev. B **71**, 205203 (2005).